Magnetorheological Damper With Variable Displacement Permanent Magnet for Assisting the Transfer of Load in Lower Limb Exoskeleton

Jiyuan Song, Aibin Zhu, *Member, IEEE*, Yao Tu, Chunli Zheng, and Guangzhong Cao, *Senior Member, IEEE*

***Abstract*— Magnetorheological (MR) fluid exhibits the ability to modulate its shear state through variations in magnetic field intensity, and is widely used for applications requiring damping. Traditional MR dampers use the current in the coil to adjust the magnetic field strength, but the accumulated heat can cause the magnetic field strength to decay if it works for a long time. In order to deal with this shortcoming, a novel MR damper is proposed in this paper, which is based on a variable displacement permanent magnet to adjust the output resistance torque and applied to an exoskeleton joint for human load transfer assistance. A finite element model is used to determine the size parameters of the magnet and separator, so that the maximum output torque is optimal and the torque is uniformly distributed with the magnet displacement. The MR damper was characterized and calibrated on the experimental bench to make it controllable. The novel design enables the torque mass density of the MR damper to reach 8.83Nmm/g, the torque volume density to reach 48.7N/mm^2, and has stability for long-term operation. Based on the torque control method proposed, a preliminary human experiment is conducted. The ground reaction force (GRF) data of the subjects is analyzed here, which represents the effect of load transfer to the exoskeleton. Compared with no exoskeleton, the GRF with exoskeleton is significantly reduced: the peak GRF in early stance phase is reduced by 24.14%, and in late stance phase is reduced by 19.77%. Based on our net load benefit (NLB) and net force benefit (NFB) evaluation indicators, the effectiveness of the proposed MR damper exoskeleton for human weight bearing assistance is established.**

***Index Terms*— Magnetorheological (MR) damper, weight bearing, lower-limb exoskeleton, assisting efficiency.**

Manuscript received 23 December 2022; revised 19 June 2023, 20 September 2023, and 21 November 2023; accepted 26 November 2023. Date of publication 1 December 2023; date of current version 12 January 2024. This work was supported in part by the National Natural Science Foundation of China under Grant 52175061, in part by the Xinjiang Funded by Autonomous Region Major Science and Technology Special Project under Grant 2021A02002, in part by the Shaanxi Provincial Key Research and Development Program under Grant 2022SF-352, in part by the Shanxi Provincial Key Research Project under Grant 2020XXX001, and in part by the Fundamental Research Funds for the Central Universities under Grant xzd012022019. *(Corresponding author: Aibin Zhu.)*

This work involved human subjects or animals in its research. Approval of all ethical and experimental procedures and protocols was granted by the Biomedical Ethics Committee of Xi'an Jiaotong University under Application No. 2020-1025.

Jiyuan Song, Aibin Zhu, and Yao Tu are with the Institute of Robotics and Intelligent Systems, Shaanxi Key Laboratory of Intelligent Robots, Key Laboratory of Education Ministry for Modern Design and Rotor-Bearing System, Xi'an Jiaotong University, Xi'an 710049, China (e-mail: jysong@stu.xjtu.edu.cn; abzhu@mail.xjtu.edu.cn; tu1007909971@stu.xjtu.edu.cn).

Chunli Zheng is with the Department of Environmental Science and Engineering, Key Laboratory of Thermo-Fluid Science and Engineering, Xi'an Jiaotong University, Xi'an 710049, China (e-mail: clzheng@mail.xjtu.edu.cn).

Guangzhong Cao is with the Guangdong Key Laboratory of Electromagnetic Control and Intelligent Robots, Shenzhen University, Shenzhen 518060, China (e-mail: gzcao@szu.edu.cn).

Digital Object Identifier 10.1109/TNSRE.2023.3338969

I. Introduction

With the development of electromechanical systems, there have been many applications of lower limb exoskeletons in different fields to assist human movement in recent years, such as rehabilitation and weight-bearing [1], [2], [3], [4]. Different with the rehabilitation, which requires consideration of precise positioning and strong constraints on the human body, weight-bearing exoskeletons are designed for healthy individuals, so flexibility is particularly important. As for a weight-bearing exoskeleton, walking with heavy objects often occurs in military marches, industrial transportation and outdoor activities [5]. Compared with other transportation platforms, exoskeleton is favored for its advantages of concomitance and convenience.

In the state of weight bearing, the human body should not only keep standing, but also perform walking tasks. If there is no assisting equipment, the load is transferred from the back to the hip joint, knee joint and ankle joint of human lower limb [6], [7], which can lead to lower limb joint pain and other musculoskeletal diseases (MSD) [8], [9]. Therefore, carrying objects while walking can pose risks, when executed improperly or with heavy loads. Lower limb exoskeleton has a certain preventive effect on reducing the risk of MSD [10]. The assistance of exoskeleton in weight bearing and transportation is mainly reflected in that it can transfer the load to the ground to reduce the load borne by the human body in the stance

phase. Some devices have been successful in reducing the metabolic cost of the human when walking with load [7], [11].

In terms of the lower limbs of the human, the knee joint torque in the sagittal plane is shown in Fig. 4(c), which is the moment curve after the standardization of the subject's body mass. As opposed to the hip and ankle joints, the knee joint has a higher rotational peak speed (500°/s) in the swing phase [12] and a high braking torque in the stance phase [13], [14]. The knee joint mechanical power is largely negative throughout the gait cycle in the human walking [15], which is because the joint torque and direction of motion are opposite in the support phase, especially at slow walking speeds. In this case, if the active actuator [2], [16], [17] is used in the assisting equipment, the motor is required to work in plug braking mode, and will consume high power from the batteries for braking, which is neither energy-saving nor safe [18]. In order to give consideration to the load performance and portability of the actuator, it may not be desirable to rely entirely on motor braking for the human gait assistance. Some researchers focus on the passive [19] or semi-active devices to assist the human body. Semi-active devices equipped with magnetorheological (MR) damper have also been developed to provide controllable and effective braking for exoskeletons and orthotics [20], [21], [22]. MR fluid is an intelligent material whose rheological properties can be changed [23]. In the absence of a magnetic field, the particles in its material are uniformly distributed, and behave as Newtonian fluid; When in a magnetic field, the particles are magnetized and form a chain structure, generating mechanical resistance against the movement of the shear surface.

Based on MR fluid, A MR damper is widely used in many fields, such as shock absorption and deceleration, because of its fast response time, high torque volume ratio, low power requirements, and low turn off friction. A MR device attached to the knee joint can increase damping during heel impact and early stance-phase, preventing knee joint flexion during weight application. In order to improve the torque output performance of MR damper, many researchers have attempted optimization work and achieved preliminary effective results. Kikuchi and Kobayashi [24] designed a rotating MR damper with multi coil structure to improve the magnetic field performance. Zhu [25] designed a low torque disc MR damper. In order to increase the effect of drag torque, Senkal and Gurocak [26] developed a MR damper with serpentine flux path. Hamid and Sayyaadi [27] designed a MR damper with T-shaped drum. Yu et al. [28] designed a new rotating MR damper based on spiral flow. Wei et al. [29] proposed a high torque rotating MR damper with parallel plate channels. However, the way to generate and adjust the magnetic field in these traditional MR dampers [24], [25], [26], [27], [28], [29] is to change the current in the coil, so as to achieve the output damping change of the MR damper joints, as shown in Fig. 1(a). Although this method is convenient, long time operation will cause serious heating of the coil, which will lead to the attenuation of the magnetic field strength and affect the damping torque adjustment performance. It is a common method to increase the theoretical maximum output torque of MR dampers by changing the magnetic flux path [30]. However, due to the

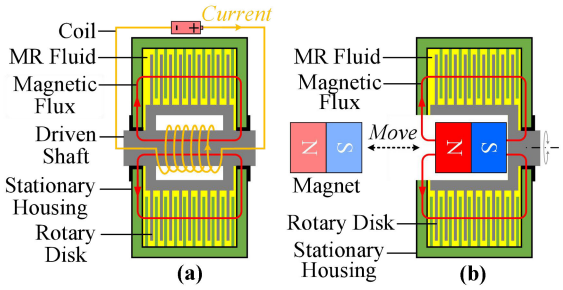

Fig. 1. The principle of traditional and the proposed magnetorheological (MR) dampers. (a) The principle of traditional MR damper which is based on coil current; (b) The principle of proposed MR damper in this paper which is based on variable displacement permanent magnet.

narrow space inside the MR damper, an excessively thin wire diameter will cause significant heating of the coil, which limits the current input and limits the maximum torque density of the MR damper. Therefore, it is imperative to devise novel magnetorheological (MR) dampers capable of meeting the requirements for high torque output and prolonged operational durability.

In this article, we created a small MR brake, which is an upgrade based on our previous generation's research [31]. The difference is that the MR damper proposed in this paper uses a variable displacement permanent magnet to adjust the magnetic field intensity, as shown in Fig. 1(b). The position of the permanent magnet in the joint cavity can be adjusted by controlling a small motor, and the state of the magnetic fluid in the joint can be changed to achieve the adjustment of the joint damping torque. Compared with the traditional coil type MR damper, the MR damper proposed in this paper improves the principle of magnetic field intensity adjustment. Specifically, adjusting the displacement of the permanent magnet instead of adjusting the current in the coil to adjust the magnetic field intensity. The magnetic field intensity of the permanent magnet with high magnetizing amount is superior than that of the coil, which improves the maximum torque density of the MR damper. At the same time, its shape is suitable for the assembly of joints. Its most remarkable feature is that it can be used for a long time without torque attenuation due to coil heating. The segmented parameters of the permanent magnet are optimized to make the magnetic field intensity change uniformly and facilitate the linear control accuracy.

The torque output performance is characterized by the bench experiments. Based on the segmented permanent magnet module and magnetic circuit optimization design, the maximum output torque of the proposed MR damper can reach 6.47Nm, i.e. the torque mass ratio (TMR) and the torque volume ratio (TVR) is 8.83 Mmm/g and $48.7{*}10^{-3}$N/mm^2. In addition, this paper also proposes a control strategy, which is based on the position loop to control the output torque of the MR damper. The MR damper is assembled in the knee joint of a passive lower limb exoskeleton, and with the human gait phase recognition method [32] previously proposed, the assisting effect of the weight bearing ability was tested by a preliminary human experiment. Based on the collected plantar pressure and motion information, the data significance of ground reaction

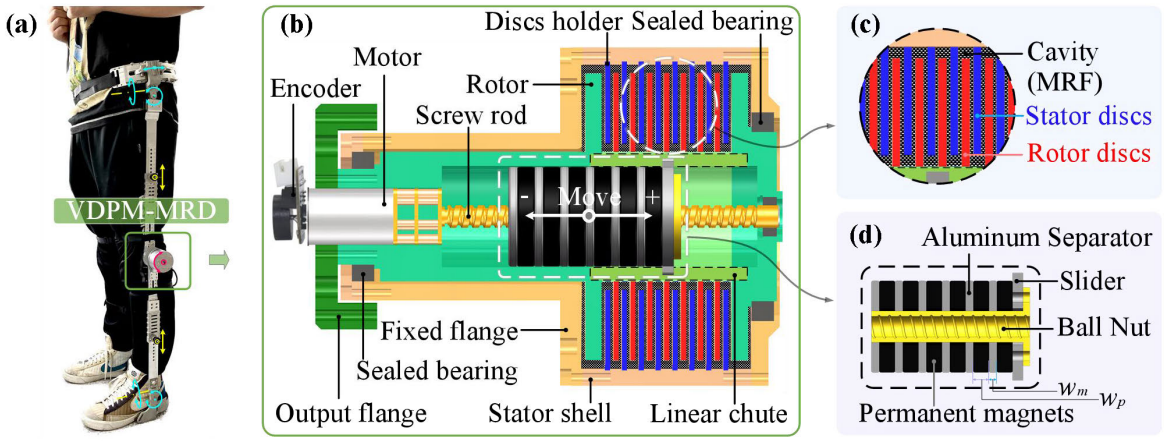

Fig. 2. Overview of the magnetorheological damper (MR damper) based on variable displacement permanent magnet for the knee joint of lower limb exoskeleton. (a) Prototype exoskeleton with the proposed MR damper knee joint. In addition to the knee joint equipped with MR damper, the hip joint and ankle joint each have 3 and 2 degrees of freedom, with full flexibility; (b) Detailed design display of the MR damper. The green is the rotor, and the brown is the stator. The MR damper consists of a set of permanent magnet module, which can be driven by the motor-screw-nut mechanism to adjust the magnetic strength of the multi-discs stacking area; (c) Multi-discs stacking area, red discs are connected to the rotor and blue discs are connected to the stator; (d) The permanent magnet module with ball nut and slider. Multiple permanent magnets and aluminum sheets are stacked on the nut alternately. The slider can slide in the chute area in the rotor.

force (GRF) of the human with and without exoskeleton was compared. Based on our net load benefit (NLB) and net force benefit (NFB) indicators, we evaluated the assisting efficiency of the exoskeleton. The maximum NLB is 41.00%, and the maximum NFB is 30.25%.

The remaining sections of this article are as follows. Section II introduces the design principles of the proposed MR damper, including the mechanical design, the model parameter optimization and the controller design. Section III presents the experimental procedure and data analysis of the results, including the MR damper performance characterization experiment and exoskeleton wearing experiment. Section IV is the discussion. Finally, Section V summarizes the conclusions of this paper.

II. MR Damper Design

A. Overall Mechanical Design

The proposed magnetorheological (MR) damper is used for load transfer of exoskeleton, which is installed on the knee joint of the exoskeleton. As shown in Fig. 2(a), except for the knee joint, the hip joint and ankle joint each have 3 and 2 degrees of freedom (DOF) respectively, which satisfies the free movement of human joints. As shown in Fig. 2(b), MR damper has two main components: rotor and stator ring. Discs are embedded and installed on the rotor and stator ring with cyanoacrylate adhesive respectively, and they are staggered and overlapped. The weight of the MR damper is 741g. The rotor (green) and discs (red/blue) are magnetic conductive materials (DT4C, which is pure iron material) [24], [25], [26]. The shell (brown) is non-magnetic material (6061 aluminum alloy). The cavity between rotor discs and stator discs is filled with magnetorheological fluid (MRF). Since the relative permeability of low carbon steel (DT4C) is higher than that of aluminum, the magnetic field lines are often concentrated in the steel with high magnetic permeability rather than the aluminum with low magnetic permeability. Sealed bearings are used between the rotor and the housing and set with proper clearance so that the torque in the magnetic field free state can be ignored. As shown in Fig. 2(c), each disc in the multi-discs area is fixed circumferentially by a dovetail structure and axially by a gasket. The thickness of the gasket can be changed to adjust the fluid gap between the rotor discs and stator discs. In addition, a rectangular groove is arranged at the shell to facilitate the injection of MRF. To ensure that there is no fluid leakage, silicone pads are applied between the mating surface of the housing and the end cap.

The proposed MR damper rotor uses permanent magnet as the effector of the magnetic field, which is completely different from most of the schemes using coils. The transmission of permanent magnet module is installed inside the rotor. Because of the design decision to incorporate the permanent magnet into the rotor, the permanent magnet and the rotor must remain stationary while the stator housing rotates around it to keep the wires from twisting. As shown in Fig. 2(d), the nut-slider mechanism and the permanent magnet unit are fixed together, and the permanent magnet can move axially with the drive of the motor-screw mechanism to adjust the magnetic field intensity in the multi-discs area.

B. Model Parameter Optimization

The magnetostatic module of finite element (FEM) software (ANSYS, Inc. Canonsburg, PA, USA) was used to model and iteratively improve the MR damper design. The magnetic field effect can be directly obtained by inputting the material of the permanent magnet (NdFe35). Note that the permanent magnet is separated by a number of aluminum separator sheets (Fig. 2(d)) to keep the magnetic field intensity gradually increases when it gradually enters the multi-disks area, which is conducive to accurate control. The most important characteristic to evaluate MR damper is torque volume ratio (TVR). The total length of the permanent magnet is 29 mm, the outer diameter R_1 and inner diameter R_2 are 17.5 mm and 6 mm respectively, the thickness of the separator sheet and the single magnetic disc are w_p and w_m respectively, and the

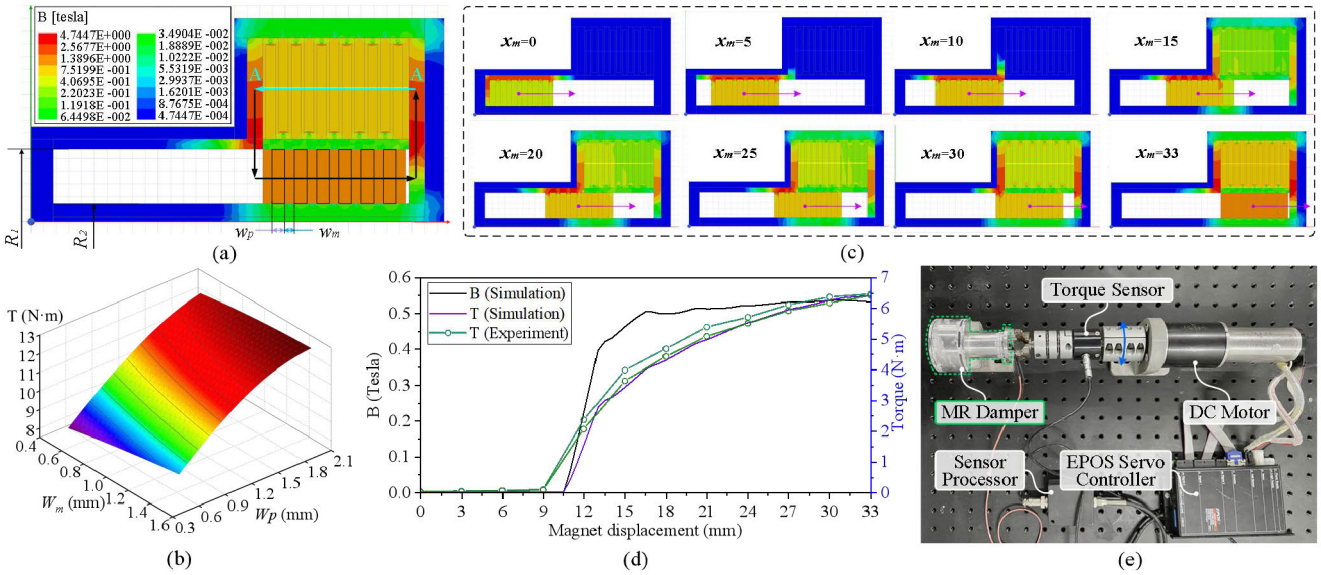

Fig. 3. Size optimization and performance characterization of the MR damper. (a) Maximum magnetic field state of disks stacking area; (b) The influence of the thickness of permanent magnet and separator on the output torque of MR damper; (c) Visualization of MR damper magnetic field intensity corresponding to different displacement of permanent magnet; (d) The magnetic field intensity and output torque of the MR damper disks stack area vary with the displacement of the permanent magnet; (e) The experimental device for testing braking torque of the MR damper. The test bench consists of a DC motor connected to the MR damper and a torque sensor for capturing brake torque.

number of rotor discs and stator discs in the multi-discs area is N respectively. Therefore, when the maximum volume is determined by the exoskeleton joint, parameters w_p and w_m are optimized to obtain the best magnetic field effect.

The magnetic flux density determines the shear stress generated by MRF. Shear stress can be obtained from Bingham viscoplastic model. From [39], the relationship between sheer stress τ_r and magnetic flux density B can be expressed as (1).

$$\tau_r = -117.54B^3 + 120.14B^2 + 21.18B - 0.115 \quad (1)$$

The torque output T of the multi-disks area can be described as follows.

$$T = \frac{2\pi}{3}(2N-1)(R_1^3 - R_2^3)\tau_r \quad (2)$$

All materials, including magnets (NdFe35), B-H curves of MRF-122EG and DT4C, are input into the software. Set boundaries and incentives. Magnetic flux density B can be calculated by Ansys Maxwell. In the model, several points are printed at the center of each facet, which represent the average magnetic flux density. Obtain the magnetic flux density of the point in the magnetic field calculator and substitute its value into (1) and (2). The torque obtained is shown in Fig. 3(b). The optimal parameters of w_p and w_m are determined to be 2mm and 1.2mm respectively. Magnetic field state of MR damper corresponding to different positions of permanent magnet is shown in Fig. 3(c), magnetic flux density B (black) and output torque T (purple) of A-A facet are shown in Fig. 3(d).

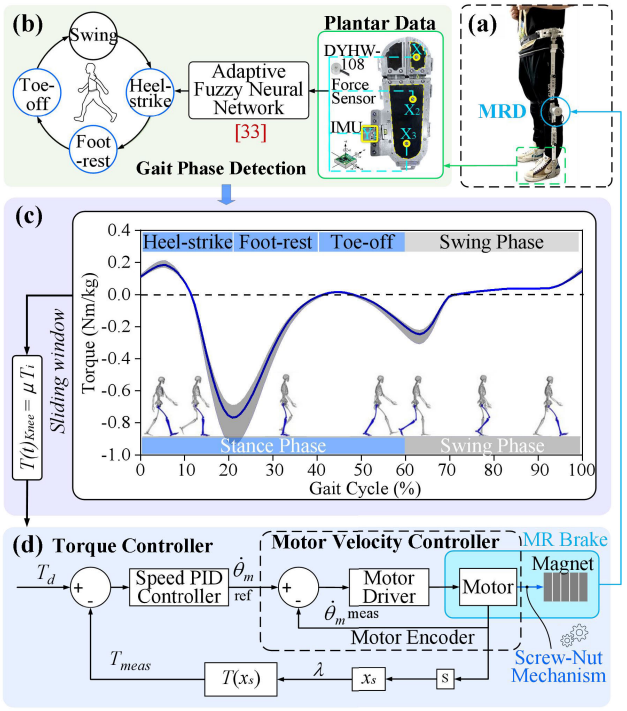

Fig. 4. Overview of the real-time control scheme. (a) The complete system worn by the subject; (b) Gait phase recognition method; (c) Knee joint moment curve during walking standardized according to the subject's weight, The thick line and the shaded area show the mean and the standard deviation for the target dataset; (d) Torque controller of the MR damper.

C. Controller Design

In the MR damper, the hall encoder at the end of the motor is used to measure the displacement of the slider x_s, the acquisition frequency of the encoder is 100Hz. According to (3), the output torque of MR damper can be estimated in real time. This method does not require additional torque sensor, which can make the actuator more compact. Fig. 4(d) shows the torque control block diagram, which consists of two cascade control loops. The speed of the motor in the inner ring

is controlled by the modulation signal of the motor driver in the speed mode.

The displacement of magnet slider can be used to characterize the output torque of MR damper.

$$T_s = \lambda(x)x_s \tag{3}$$

where x_s is the displacement of the magnet slider; T_s is the output torque of the MR damper; $\lambda(x)$ is the conversion coefficient from magnet displacement to output torque, which can be obtained from the torque displacement curve in Fig. 3 (d). In the transparent mode, $x_s = 0$. In the damper torque mode, just move the magnet to output the desired torque.

In this paper, assistance was generated based on the gait phase detection, which were synchronized with the human joint kinematics. A gait cycle (GC) includes the stance phase and the swing phase. In detail, the stance phase includes the heel-strike (HS), foot-rest (FR) and toe-off (TO).

Here, the adaptive neuro fuzzy inference system (ANFIS) is used for gait phase division, which is a fuzzy inference system based on the Takagi Sugeno model in our previous work [32]. The plantar pressure data and IMU data are fused to achieve smooth, continuous and accurate gait phase detection. The gait recognition method used is shown in Fig. 4(b). The torque-time relationship here is based on the normalized human gait curve (Fig. 4(c)), which is obtained by subjects walking on a three-dimensional force measuring board (AMTI), with motion capture system (Vicon) to record the trajectory of human limb motion, and calculated by inverse dynamics. As the output torque of MR damper is limited, it is adjusted to 10% of the curve in proportion i.e., the μ is set to 0.1, and the torque value is interpolated and continuous.

III. Experiment Evaluation and Results

This section is to characterize the performance of the proposed MR damper, and to test the exoskeleton assisting effect for the human weight bearing. In subjects experiments, the assisting efficiency of exoskeleton is calculated by the biomechanical effects of exoskeleton and load conditions on the human. The ground reaction force (GRF) of participants with and without exoskeleton was analyzed, which represents the effect of load transfer of exoskeleton.

A. Torque Characterization of the MR Damper

To test the performance of the relationship between braking torque and magnet displacement of the MR damper, we created a test bench device (see Fig. 3 (e)). The shell of the MR damper is fixed on the test bench. We connect a brushless motor (Maxon, EC 40) to the torque sensor and the output of the MR damper in turn. We used ESCON 50/5 servo controller to drive the micro motor of MR damper. The experiment aims to characterize the output braking torque of the MR damper and establish the relationship between the position of the magnet and the output torque. Control the micro motor of the MR to drive the screw-nut mechanism, and test the braking torque of MR damper with the displacement range of the magnet-slider from 0 to 33mm at 3mm intervals. The motor (Maxon, EC 40) on the test bench starts from standstill until it breaks free from the constraints of the MR damper, and records the data of the torque sensor at this time i.e. the torque output by MR of the current permanent magnet position. The results are shown in Fig. 3(d). When the slider is at the 0 mm position (transparent state), the friction torque is about 0.06 Nm. This can be attributed to the friction between the shaft and bushing and the MR fluid. However, the rotor can rotate freely without excessive friction, which indicates that there is no contact between the rotor and the housing. With the magnet slider gradually enters the multi-disks stacking area, it shows the torque controllability of the proposed MR damper. When the magnet slider position is less than 9mm, the output braking torque of the MR damper is close to 0; When the displacement of the magnet slider is between 9 and 33 mm, the MR damper can output torque effectively. At 33mm, the MR damper is at the maximum braking torque limit (~6.47Nm), i.e. the magnetic flux density in the multi-discs stacking area is close to full magnetic saturation.

B. Preliminary Wearing Experiment

1) Experimental Protocol and Data Acquisition: The proposed MR damper is installed in the knee joint of the non-powered lower limb exoskeleton (Fig. 2 (a)). Subjects wear the exoskeleton with a backpack to load heavy objects. There is a physical interface for fixation between the carbon fiber frame of the backpack and the exoskeleton waist frame. Compared with the weight bearing of subjects without exoskeleton, the influence of weight bearing of subjects with exoskeleton is evaluated from two aspects: the human GRF and maximum weight bearing mass.

Participants were tested in 7 load conditions with and without exoskeleton, including 0kg, 5kg, 10kg, 15kg, 20kg, 25kg and 30kg. The load condition is achieved by increasing or decreasing the number of standard sandbags (5kg) in the backpack. For the without exoskeleton condition, subjects carry the backpack on the shoulder; For with the exoskeleton condition, the back plate frame of the backpack is connected with the waist frame of the exoskeleton (Fig. 5). Six healthy subjects (all male, age: 23.5 $\pm$ 2.5 years, height: 169.3 $\pm$ 6.2 cm, weight: 69.5 $\pm$ 10.5 kg) with no history of lower-limb joint injury volunteered to participate in the study with informed consent. The research design and scheme have been approved by the biomedical ethics committee of Medical Department of Xi'an Jiaotong University.

The GRF of participants was measured by the Pedar-X plantar pressure insole (Novel, Germany), and the average GRF was monitored at a frequency of 100 Hz. Note that when without the exoskeleton, the pressure insole measures the force data between the participant's sole and the ground; When with exoskeletons, it measures the force data between the participant's sole and the exoskeleton sole. All subjects walking experiments were conducted on a treadmill at a constant speed, which is set at 1.2m/s.

2) Data Processing: The purpose of this article is to design an exoskeleton with a MR damper to assist the human body to transfer the load to the ground in weight-bearing walking process. When the human carry a load on the back with exoskeleton, the coupling model is shown in Fig. 6. The GRF of the feet includes vertical and horizontal components [33] (Fig.6 (c)) in the gait cycle. The vertical component of the

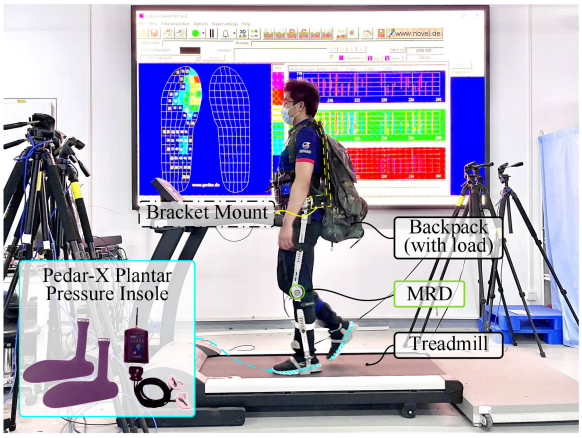

Fig. 5. Subjects wear test scenarios. Participants wore exoskeleton to walk on the treadmill. The light backpack on their back and the waist of exoskeleton had a physical interface. The plantar pressure data is measured by the Pedar-X planter pressure insole.

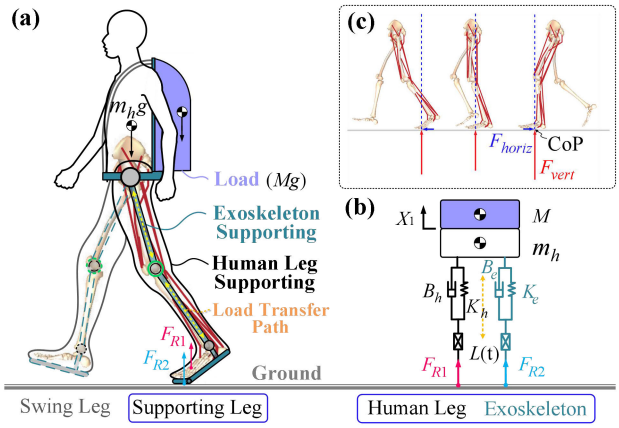

Fig. 6. The model of the human body when walking with a load while wearing an exoskeleton. (a) Human-exoskeleton coupled model for transferring load to the ground; (b) A simple model which can approximate the vertical dynamics of the human body while walking with a load; (c) The vertical and horizontal components of the GRF in the gait cycle.

GRF is widely used as a measure of weight bearing efficiency of the exoskeleton [34], [35]. Here, the foot mechanism [36] of the exoskeleton is with an elastic metal sheet and soft rubber at the bottom, and there is a hinge mechanism at the toe joint. Therefore, insole forces were measured by the pressure insoles to estimate the vertical GRF of the human participant.

Furthermore, the model is simplified as a vertical mass oscillator model with the coupling equation shown below, where the linear model of subject's leg is defined by its damping coefficient B_h and stiffness coefficient K_h. Similarly, the corresponding parameters $\{B_e, K_e\}$ are used to define the exoskeleton model. $L(t)$ is a function of the linear leg length, which is a variable parameter over time to achieve motion similar to the vertical centroid displacement of subjects. m_h is the mass of subjects. F_{R1} and F_{R2} are the vertical component of GRF of subject and exoskeleton respectively.

$$(K_h + K_e)(X_1 - L(t)) + (B_h + B_e)(\dot{X}_1 - \dot{L}(t)) + (m_h + M_1)g = F_{R1} + F_{R2} \quad (4)$$

When the human carries a load without exoskeleton, the linear equation of motion is given by:

$$K_h(X_1 - L(t)) + B_h(\dot{X}_1 - \dot{L}(t)) + (m_h + M_2)g = F_{R1} \quad (5)$$

where M_1 is the load weight when the human with exoskeleton and M_2 is the load weight when the human without exoskeleton.

When the vertical component of GRF of subjects F_{R1} in (4) and (5) is the same, the variation of M_1 and M_2 can characterize the benefits of exoskeleton for weight bearing transfer tasks. The weight bearing assisting efficiency (AE) used to quantify the exoskeleton is defined as follows.

$$\text{AE}[\%] = \frac{M_1 - M_2}{M_1} \times 100\% \quad (6)$$

The GRF measured perpendicular to the plantar pressure center is passed through a 5Hz low-pass filter, and the gait cycle time is expressed as a percentage. The stance phase in the gait cycle is divided into early stance and late stance. Extract the measured GRF data of 20 consecutive gait cycles, i.e., 20 times from the left heel strike to the next left heel strike for analysis. Statistical analyses were performed using SPSS 25.0 (SPSS Corporation, Chicago, Illinois, USA). The variables of GRFs were analyzed using two factor repeated measures ANOVA, including two kinds of conditions (with and without exoskeleton) and seven levels of load (0kg, 5kg, 10kg, 15kg, 20kg, 25kg, and 30kg). The p value was set at 0.05. Every significant ANOVA result was tracked by t-test, which was adjusted by the Bonferroni method. Curve regression was used to fit the function of plantar pressure and load.

As shown in (4) and (5), the human body's GRF F_{R1}increases with the increase of the load mass. In order to evaluate the indicators of positive effects of the exoskeleton on subjects, the following two aspects can be analyzed respectively:

In the weight-bearing event, when the GRF of the subject with exoskeleton is equal to that without exoskeleton, the net load benefit (NLB) percentage of assisting efficiency of exoskeleton in weight bearing task is proposed as (7), which is based on (6).

$$\text{NLB}[\%] = \frac{Load_{Exo} - Load_{NoExo}}{Load_{Exo}} \times 100\% \quad (7)$$

where the $Load_{Exo}$is the load mass of subject wearing exoskeleton, and the $Load_{NoExo}$is the load mass of subject without wearing exoskeleton.

In addition, with the load transfer of exoskeleton, the GRF of subjects is reduced. When the load mass of subject wearing exoskeleton is equal to that of not wearing exoskeleton, net force benefit (NFB) percentage (8) is also proposed.

$$\text{NFB}[\%] = \frac{F_{R1_{NoExo}} - F_{R1_{Exo}}}{F_{R1_{NoExo}}} \times 100\% \quad (8)$$

where the $F_{R1_{Exo}}$is the GRF of subject wearing exoskeleton, and the $F_{R1_{NoExo}}$is the GRF of subject without wearing exoskeleton.

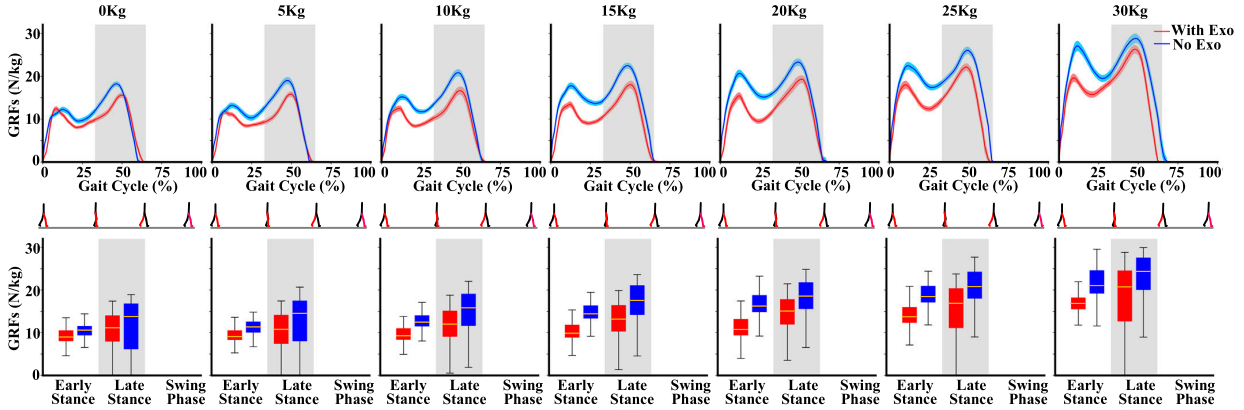

Fig. 7. Experimental results. The results of GRFs with and without exoskeletons under different load conditions showed that the GRFs of all participants with exoskeletons decreased significantly in the early and late stance compared with those without exoskeletons. Lines are medians, the gray boxes cover between the 25th to 75th percentiles of gait cycle represent the stage of the late stance phase.

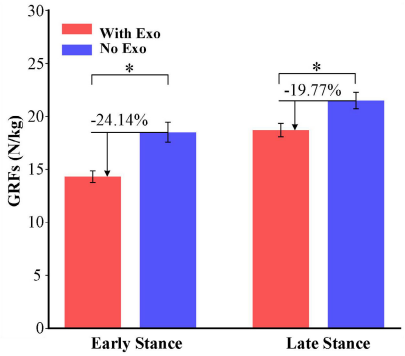

Fig. 8. Impact of exoskeleton equipment conditions on results. The peak GRFs of load carriage at 0 - 30kg, bars represent early stance and late stance with wearing the exoskeleton (Exo), without wearing the exoskeleton (No Exo). Asterisks indicate statistically significant differences.

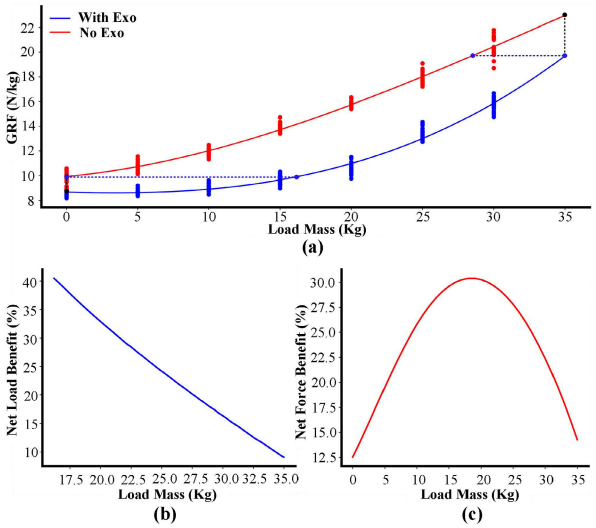

Fig. 9. Assisted efficiency results. (a) The linear relationship between the average resultant moment of load and support when all participants wore exoskeleton and did not wear exoskeleton; (b) The relationship between exoskeleton load and net load benefit; (c) The relationship between exoskeleton load and net moment benefit.

3) Data Analysis Results:

a) GRFs: As shown in Fig. 7, wearing exoskeleton or not and load levels have certain influence on the experimental results. In the swing phase, the GRF did not show major effects of the exoskeleton equipment and load because the foot did not touch the ground. As shown in Fig. 8, compared with no exoskeleton, the peak GRF of subjects with exoskeleton is significantly reduced (p <0.05): the peak GRF in early stance phase is reduced by 24.14%, and in late stance phase is reduced by 19.77%. For the impact of the load, the peak GRF of overall stance phase increases significantly with the increase of the load mass. However, there was no significant difference between the GRF values of 0kg and 5kg in late GRF. The analysis of stance phase duration in gait cycle did not reveal significant between exoskeleton equipment and load levels. No significant major effects of equipment and load were obtained, but for some load levels, the GRF of stance duration was significantly different from others. For example, for 0 kg and 5 kg loads, although the GRF is no significant difference, it is significantly lower than the value of other load levels; The GRF values of 10kg and 15kg have no significant difference, but are significantly higher than those of other load levels. And the GRF is no significant difference among the load of 10kg, 25kg and 30kg.

b) Assisted efficiency evaluation: For with and without exoskeleton conditions, the fitting relationship between the average GRF and the load mass during the stance phase of the gait cycle is shown in Fig. 9(a). The two fitting lines of with and without exoskeleton are significantly different. The fitting line of the GRF with exoskeleton are lower than those without exoskeleton. According to (7) and (8), plot the relationship between net load benefit (NLB) percentage and net force benefit (NFB) percentage and load levels, as shown in Figs. 9(b) and 9(C).

As shown in Fig. 9(b), within the effective calculation range (16kg∼35kg), the percentage of NLB decreases significantly with the increase of load mass. The NLB percentage of the 16kg load condition is the highest, which is 41.00%; The NLB percentage of the 35kg load condition is the lowest, which is 7.73%. As shown in Fig. 9(c), within the effective calculation range (0kg∼35kg), the percentage of NFB first increases and then decreases with the increase of load mass. For the 0kg and 35kg load condition, the NFB percentage is 12.50% and 14.15%, respectively; For the 20kg load condition, the NFB percentage is the highest, 30.25%.

IV. Discussion

This work characterized the benefits of the MR damper through modeling and experiments, the proposed design result in a high torque density MR damper and the output torque is controllable by moving the displacement of the permanent magnet. Based on the NLB and NFB indicators, the exoskeleton with the MR damper knee actuator was evaluated, which indicates the effectiveness of weight bearing.

A. Performance Advantages of the MR Damper

The MR damper proposed in this paper is based on a novel magnetic field regulation method, i.e., the output torque can be adjusted by changing the position of the permanent magnet in the multi-disks stacking area. The traditional MR damper adjusts the output torque by changing the current in the coil [30], [37], [38], [39], which has a disadvantage of being easy to heat and is not conducive to long time operation, because the magnetism will decay with the increase of temperature. Within the movable range of the magnet slider (0∼33 mm), the effective output torque range is (9 mm∼33 mm), accounting for 72.73% of the maximum range. Based on the segmented permanent magnet module and magnetic circuit optimization design, the maximum output torque of the proposed MR damper can reach 6.47Nm, i.e., the torque mass ratio (TMR) and the torque volume ratio (TVR) is 8.83 Nmm/g and $48.7*10^{-3}$N/mm^2, which is higher than the state-of-art [30], [37], [38], [39], as shown in Table I. It indicates that the permanent magnet scheme has the potential to output large torque in MR damper, which is the main advantage over the coil scheme. And with the development of magnetizing technology, it will show better performance. Compared with [39], the TMR of the MR damper proposed in this paper is higher than 89.5% of [39], while TVR is only higher than 20.5% of [39]. The reason why the volume advantage is not obvious is that the screw-nut mechanism occupies part of the space and needs to reserve the space for the movement of permanent magnet. Due to the friction of the rotor, when the magnet-slider is at the farthest position from the multi-disk stacking area, the output torque is 0.06 Nm (less than 0.9% of the maximum output torque). This ensures the feasibility of minimizing the constraints on the wearer of the exoskeleton in the "zero torque mode".

B. Subjects Tests Response and Interpretations

Based on the proposed torque controller with the gait phase recognition method we have developed, the MR damper was assembled at the knee joint of a passive lower limb exoskeleton, and subjects wore the exoskeleton for weight bearing assistance testing. With the assisting efficiency evaluation method proposed by us, the GRF data of subjects are collected to measure the NLB and NFB of exoskeleton for the human in the weight bearing task.

It can be seen from the reduction of subjects GRF when wearing exoskeleton (Fig. 9(a)) that the exoskeleton can undertake part of the transmission of weight mass in weight bearing event. As for the assisted efficiency of the exoskeleton, it is discussed from two aspects (NLB and NFB): As the weight of the load mass increases, NLB gradually decreases (Fig. 9(b)). Under the condition that the subjects reach the same GRF, the greater the load mass, the smaller the advantages of exoskeleton bearing transfer. As the weight bearing mass increases, NFB first increases and then decreases (Fig. 9(c)). Under the same load conditions, within the weight range of 0-20kg, the larger the load mass, the greater the effect of reducing GRF; Within the weight range of 20-35kg, the larger the weight, the smaller the effect of reducing GRF. If the weight bearing mass increases infinitely, as shown in Fig. 9(a). When the two curves in intersect, the exoskeleton loses its effect of assisting load transfer.

The results show that the proposed MR damper-based exoskeleton can reduce the GRF of subjects when load heavy objects and improve the ability of subjects carrying heavy objects. For the dynamics and gait phases, we found that the average GRF of subjects increased significantly with the increase of the load mass, whether in the early or late stance phase, whether with exoskeleton or not, as shown in Fig. 10(a). These are the same as the point proposed by Lloyd and Cook [40], i.e., the increase of vertical GRF is proportional to the increase of load mass. In this study, the average GRF of subjects with exoskeleton was significantly lower than that of subjects without exoskeleton for all load conditions, whether in the early or late stance phase. In terms of the stance duration, there was no significant difference between with or without exoskeleton conditions when the load was less than 10kg. This indicates that the proposed exoskeleton prototype has almost no constraints on the flexibility of subjects in low load conditions, as shown in Fig. 10(b). If the load mass is less than 15kg, the stance duration with the exoskeleton condition is longer than that without exoskeleton. But if the load is more than 30kg, the stance duration with the exoskeleton is shorter than that without exoskeleton. For the condition of subjects without exoskeleton, the stance duration increases significantly with the increase of load mass, which means that the swing duration is shorter. For the condition of subjects with exoskeleton, the stance duration won't change significantly with the increase of load. The reason is that when participants wear exoskeleton for weight bearing, part of the load is borne by exoskeleton, so that the gait of participants is less affected by the load mass. Gottschall and Kram [41] believed that the large vertical component of GRF was the main reason for the increased risk of lower limb injury. Therefore, the proposed exoskeleton has the possibility of reducing the risk of MSD.

C. Limitations of the Study

Here, we note some limitations of this study. First, the misalignment of the exoskeleton and the human joint, which is a common issue for rigid exoskeletons. The length of the thigh and calf can be adjusted to alleviate this problem, and this scheme is demonstrated in [42]. Second, the exoskeleton may increase the inertia of subjects' legs, but the passive exoskeleton is only 3.2 kg, which has less impact than the powered exoskeleton [1], [2]. Furthermore, all the subjects used the determined moment curve in the weight bearing experiment, it is a challenge to determine the torque generator suitable for everyone. Finally, in the assistance efficiency evaluation experiment section, pressure insoles were used to estimate the vertical GRF of the subjects. The line of the GRF from the

TABLE I
PERFORMANCE COMPARISON OF DIFFERENT MR DAMPER

MR damper	Paradigm	Type/Architecture	Torque (Nmm)	Mass (g)	Volume (mm^3)	TMR (Nmm/g)	TVR*10^{-3} (N/mm^2)
This work	Permanent Magnet	Multi-Disk	6470	741	132822	8.83	48.7
Patrick [30]	Coil	Inverted Hybrid	462	68	16445	6.79	28.1
Jonathan [37]	Coil	Drum	189	84	8836	2.25	21.4
Qin [38]	Coil	Multi-Drum	403	105	14470	3.84	27.9
Qin [39]	Coil	Multi-Disk	1080	232	26700	4.66	40.4

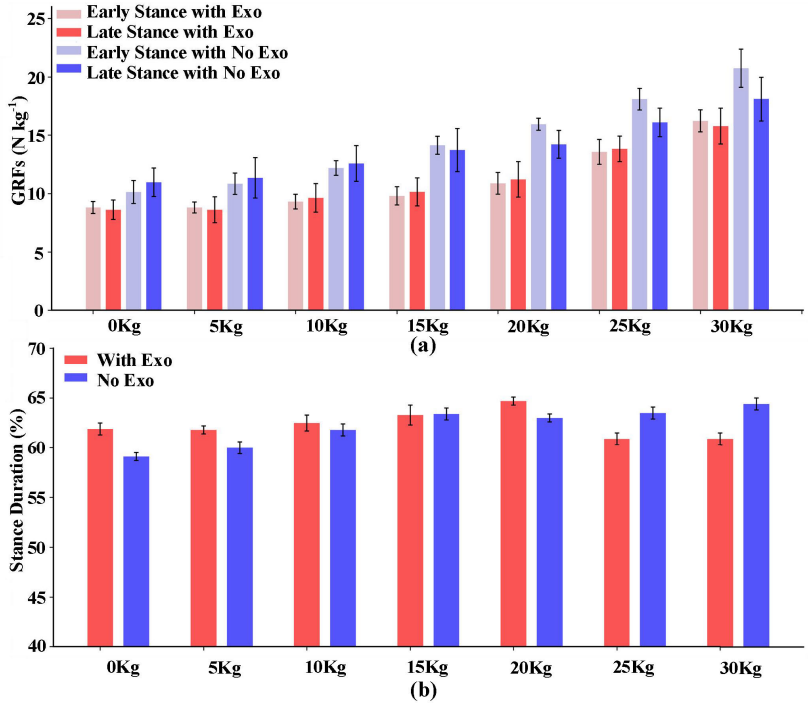

Fig. 10. Preliminary wearing experimental results in different load levels. (a) The change of GRFs of wearer with and without exoskeleton in early stance and late stance with load levels. Error bars indicate SEM (Standard Error of the Mean); (b) The change of stance duration over a gait cycle of the wearer with and without exoskeleton with load levels. Error bars indicate SEM.

experiment is not always vertical as shown in Fig 6. But it may not matter achieving the objective of the exoskeleton, and this evaluation method is widely used [34], [35]. It is worth mentioning that the MR damper exoskeleton based on the variable displacement permanent magnet proposed in this study can enhance the weight bearing ability of subjects, which is related to reducing subjects GRF.

D. Future Work

In the future work, we will try to combine the MR damper proposed in this paper with the series elastic actuator (CS-SEA) [43] we have developed, so that the actuator can balance the advantages of the compliance interaction and the load transfer performance. In addition, the TMR and TVR of the MR damper need to be adjusted to match the best fit of different biological joints for comfort and efficiency. For the controller of the assisting mode, the online human torque identification method [44] will be integrated with the exoskeleton system to assist different wearers with the best torque curve.

V. CONCLUSION

In this article, we presented a novel MR damper, which can adjust the output resistance torque based on the variable displacement of the magnet. The output characteristics of the MR damper joint were characterized by optimization design and experimental calibration. Furthermore, the MR damper is installed in the knee joint of a passive lower limb exoskeleton. We propose a real-time control method of MR damper based on gait phase recognition. In order to verify the effectiveness of MR damper exoskeleton for the human weight bearing assistance, the preliminary subjects experiments were carried out. Based on the collected plantar pressure information, the data significance of GRF of subjects with and without exoskeleton was compared. Finally, based on the NLB and NFB indicators, we evaluated the exoskeleton, which indicates the effectiveness of the proposed MR damper.

REFERENCES

[1] R. L. Hybart and D. P. Ferris, "Embodiment for robotic lower-limb exoskeletons: A narrative review," *IEEE Trans. Neural Syst. Rehabil. Eng.*, vol. 31, pp. 657–668, 2023, doi: 10.1109/TNSRE.2022.3229563.

[2] C. Meijneke et al., "Symbitron exoskeleton: Design, control, and evaluation of a modular exoskeleton for incomplete and complete spinal cord injured individuals," *IEEE Trans. Neural Syst. Rehabil. Eng.*, vol. 29, pp. 330–339, 2021, doi: 10.1109/TNSRE.2021.3049960.

[3] R. Nasiri, A. Ahmadi, and M. N. Ahmadabadi, "Reducing the energy cost of human running using an unpowered exoskeleton," *IEEE Trans. Neural Syst. Rehabil. Eng.*, vol. 26, no. 10, pp. 2026–2032, Oct. 2018, doi: 10.1109/TNSRE.2018.2872889.

[4] A. Sutrisno and D. J. Braun, "Enhancing mobility with quasi-passive variable stiffness exoskeletons," *IEEE Trans. Neural Syst. Rehabil. Eng.*, vol. 27, no. 3, pp. 487–496, Mar. 2019, doi: 10.1109/TNSRE.2019.2899753.

[5] G. J. Bastien, P. A. Willems, B. Schepens, and N. C. Heglund, "Effect of load and speed on the energetic cost of human walking," *Eur. J. Appl. Physiol.*, vol. 94, pp. 76–83, May 2005, doi: 10.1007/s00421-004-1286-z.

[6] J. Song, A. Zhu, Y. Tu, and J. Zou, "Multijoint passive elastic spine exoskeleton for stoop lifting assistance," *Int. J. Adv. Robotic Syst.*, vol. 18, no. 6, Nov. 2021, Art. no. 172988142110620, doi: 10.1177/17298814211062033.

[7] R. L. Medrano, E. J. Rouse, and G. C. Thomas, "Biological joint loading and exoskeleton design," *IEEE Trans. Med. Robot. Bionics*, vol. 3, no. 3, pp. 847–851, Aug. 2021, doi: 10.1109/TMRB.2021.3098920.

[8] T. K. Hamzat, T. A. Abdulkareem, O. O. Akinyinka, and F. A. Fatoye, "Backpack-related musculoskeletal symptoms among Nigerian secondary school students," *Rheumatol. Int.*, vol. 34, no. 9, pp. 1267–1273, Sep. 2014, doi: 10.1007/s00296-014-2962-x.

[9] S. A. Birrell and R. A. Haslam, "Subjective skeletal discomfort measured using a comfort questionnaire following a load carriage exercise," *Mil. Med.*, vol. 174, no. 2, pp. 177–182, Feb. 2009, doi: 10.7205/milmed-d-58-7308.

[10] A. M. Dollar and H. Herr, "Lower extremity exoskeletons and active orthoses: Challenges and state-of-the-art," *IEEE Trans. Robot.*, vol. 24, no. 1, pp. 144–158, Feb. 2008, doi: 10.1109/TRO.2008.915453.

[11] W.-S. Kim, S.-H. Lee, H.-D. Lee, S.-N. Yu, J.-S. Han, and C.-S. Han, "Development of the heavy load transferring task oriented exoskeleton adapted by lower extremity using qausi-active joints," in *Proc. ICCAS-SICE*, Aug. 2009, pp. 1353–1358.

[12] S. W. Lipfert, *Kinematic and Dynamic Similarities Between Walking and Running*. 2010.

[13] D. Lim, M. D. Castillo, A. J. Bergquist, M. Milosevic, and K. Masani, "Contribution of each motor point of quadriceps femoris to knee extension torque during neuromuscular electrical stimulation," *IEEE Trans. Neural Syst. Rehabil. Eng.*, vol. 29, pp. 389–396, 2021, doi: 10.1109/TNSRE.2021.3052853.

[14] H. Ma, B. Chen, L. Qin, and W. H. Liao, "Design and testing of a regenerative magnetorheological actuator for assistive knee braces," *Smart Mater. Struct.*, vol. 26, no. 3, 2017, Art. no. 035013.

[15] V. T. Inman, H. J. Ralston, and F. Todd, "Kinetics of human locomotion," in *Human Walking*, J. Rose and J. G. Gamble, Eds. Baltimore, MD, USA: Williams Wilkins, 1981, p. 91.

[16] D. Lee, E. C. Kwak, B. J. McLain, I. Kang, and A. J. Young, "Effects of assistance during early stance phase using a robotic knee orthosis on energetics, muscle activity, and joint mechanics during incline and decline walking," *IEEE Trans. Neural Syst. Rehabil. Eng.*, vol. 28, no. 4, pp. 914–923, Apr. 2020, doi: 10.1109/TNSRE.2020.2972323.

[17] A. Martínez, C. Durrough, and M. Goldfarb, "A single-joint implementation of flow control: Knee joint walking assistance for individuals with mobility impairment," *IEEE Trans. Neural Syst. Rehabil. Eng.*, vol. 28, no. 4, pp. 934–942, Apr. 2020, doi: 10.1109/TNSRE.2020.2977339.

[18] X. Zhou and J. Fang, "Precise braking torque control for attitude control flywheel with small inductance brushless DC motor," *IEEE Trans. Power Electron.*, vol. 28, no. 11, pp. 5380–5390, Nov. 2013, doi: 10.1109/TPEL.2013.2244617.

[19] B. Zhang, T. Liu, B. Zhang, and M. G. Pecht, "Recent development of unpowered exoskeletons for lower extremity: A survey," *IEEE Access*, vol. 9, pp. 138042–138056, 2021, doi: 10.1109/ACCESS.2021.3115956.

[20] H. Ma and W.-H. Liao, "Design and analysis of a regenerative magnetorheological actuator for gait assistance in knee joint," in *Proc. IEEE Int. Conf. Robot. Biomimetics (ROBIO)*, Dec. 2014, pp. 1158–1163, doi: 10.1109/ROBIO.2014.7090489.

[21] Ç. Akalin, T. Orhanli, A. Yilmaz, and I. Sahin, "Dynamic tests of MR (magnetorheologic) damper and analysis of response characteristics in semi-active knee prosthesis," in *Proc. 25th Signal Process. Commun. Appl. Conf. (SIU)*, May 2017, pp. 1–4, doi: 10.1109/SIU.2017.7960405.

[22] M. Kennard, K. Yagi, M. Hassan, H. Kadone, H. Mochiyama, and K. Suzuki, "Variable-damper control using MR fluid for lower back support exoskeleton," *IEEE/ASME Trans. Mechatronics*, vol. 28, no. 1, pp. 579–587, Feb. 2023, doi: 10.1109/TMECH.2022.3196098.

[23] M. R. Jolly, J. W. Bender, and J. D. Carlson, "Properties and applications of commercial magnetorheological fluids," in *Smart Structures and Materials 1998: Passive Damping and Isolation*. 1998.

[24] T. Kikuchi and K. Kobayashi, "Design and development of cylindrical MR fluid brake with multi-coil structure," *J. Syst. Des. Dyn.*, vol. 5, no. 7, pp. 1471–1484, 2011.

[25] C.-S. Zhu, "Dynamic performance of disk-type magnetorheological fluid damper under alternating magnetic field," *J. Zhejiang Univ.*, vol. 40, no. 3, pp. 8–464, Mar. 2006.

[26] D. Senkal and H. Gurocak, "Serpentine flux path for high torque MRF brakes in haptics applications," *Mechatronics*, vol. 20, no. 3, pp. 377–383, Apr. 2010.

[27] S. H. Mousavi and H. Sayyaadi, "Optimization and testing of a new prototype hybrid MR brake with arc form surface as a prosthetic knee," *IEEE/ASME Trans. Mechatronics*, vol. 23, no. 3, pp. 1204–1214, Jun. 2018.

[28] J. Yu, X. Dong, and W. Wang, "Prototype and test of a novel rotary magnetorheological damper based on helical flow," *Smart Mater. Struct.*, vol. 25, no. 2, Feb. 2016, Art. no. 025006.

[29] M. Wei, X. Rui, W. Zhu, F. Yang, L. Gu, and H. Zhu, "Design, modelling and testing of a novel high-torque magnetorheological damper," *Smart Mater. Struct.*, vol. 29, no. 2, Feb. 2020, Art. no. 025024.

[30] P. S. Wellborn, J. E. Mitchell, N. J. Pieper, and R. J. Webster, "Design and analysis of a small-scale magnetorheological brake," *IEEE/ASME Trans. Mechatronics*, vol. 27, no. 5, pp. 3099–3109, Oct. 2022, doi: 10.1109/TMECH.2021.3108127.

[31] J. Zou, A. Zhu, J. Song, D. Dang, X. Zhou, and Y. Zhang, "A novel magnetorheological damper combing multi-disc and multi-drum structures," in *Proc. 19th Int. Conf. Ubiquitous Robots (UR)*, Jul. 2022, pp. 52–57, doi: 10.1109/UR55393.2022.9826257.

[32] J. Song, A. Zhu, Y. Tu, H. Mao, and X. Zhang, "Adaptive neural fuzzy reasoning method for recognizing human movement gait phase," *Robot. Auto. Syst.*, vol. 153, Jul. 2022, Art. no. 104087, doi: 10.1016/j.robot.2022.104087.

[33] R. R. Neptune and C. P. McGowan, "Muscle contributions to whole-body sagittal plane angular momentum during walking," *J. Biomechanics*, vol. 44, no. 1, pp. 6–12, Jan. 2011, doi: 10.1016/j.jbiomech.2010.08.015.

[34] M. Hao, J. Zhang, K. Chen, H. Asada, and C. Fu, "Supernumerary robotic limbs to assist human walking with load carriage," *J. Mech. Robot.*, vol. 12, no. 6, pp. 1–18, Dec. 2020, doi: 10.1115/1.4047729.

[35] P. Yang et al., "A centaur system for assisting human walking with load carriage," in *Proc. IEEE/RSJ Int. Conf. Intell. Robots Syst. (IROS)*, Kyoto, Japan, Oct. 2022, pp. 5242–5248, doi: 10.1109/IROS47612.2022.9981394.

[36] A. Zhu, J. Song, H. Shen, and Z. Shen, "Innovative design of the foot of exoskeleton robot," in *Proc. IEEE Int. Conf. Inf. Autom. (ICIA)*, Wuyishan, China, Aug. 2018, pp. 750–755, doi: 10.1109/ICInfA.2018.8812428.

[37] J. Blake and H. B. Gurocak, "Haptic glove with MR brakes for virtual reality," *IEEE/ASME Trans. Mechatronics*, vol. 14, no. 5, pp. 606–615, Oct. 2009, doi: 10.1109/tmech.2008.2010934.

[38] H. Qin, A. Song, X. A. Zeng, and S. Hu, "Design and evaluation of a small-scale multi-drum magnetorheological brake," *J. Intell. Mater. Syst. Struct.*, vol. 29, no. 12, pp. 2607–2618, 2018, doi: 10.1177/1045389X18770878.

[39] H. Qin, A. Song, and Y. Mo, "Performance evaluation of a hollowed multi-drum magnetorheological brake based on finite element analysis considering hollow casing radius," *IEEE Access*, vol. 7, pp. 96070–96078, 2019, doi: 10.1109/ACCESS.2019.2930301.

[40] R. Lloyd and C. B. Cooke, "Kinetic changes associated with load carriage using two rucksack designs," *Ergonomics*, vol. 43, no. 9, pp. 1331–1341, Sep. 2000, doi: 10.1080/001401300421770.

[41] J. S. Gottschall and R. Kram, "Energy cost and muscular activity required for propulsion during walking," *J. Appl. Physiol.*, vol. 94, no. 5, pp. 1766–1772, May 2003, doi: 10.1152/japplphysiol.00670.2002.

[42] M. K. Shepherd and E. J. Rouse, "Design and validation of a torque-controllable knee exoskeleton for sit-to-stand assistance," *IEEE/ASME Trans. Mechatronics*, vol. 22, no. 4, pp. 1695–1704, Aug. 2017, doi: 10.1109/TMECH.2017.2704521.

[43] J. Song, A. Zhu, Y. Tu, X. Zhang, and G. Cao, "Novel design and control of a Crank-slider series elastic actuated knee exoskeleton for compliant human–robot interaction," *IEEE/ASME Trans. Mechatronics*, vol. 28, no. 1, pp. 531–542, Feb. 2023, doi: 10.1109/TMECH.2022.3204921.

[44] Y. Li et al., "Dynamic parameter identification of a human-exoskeleton system with the motor torque data," *IEEE Trans. Med. Robot. Bionics*, vol. 4, no. 1, pp. 206–218, Feb. 2022, doi: 10.1109/TMRB.2021.3137970.